

CANCER

CRISPR-Cas9 genome editing using targeted lipid nanoparticles for cancer therapy

Daniel Rosenblum^{1,2,3,4*}, Anna Gutkin^{1,2,3,4*}, Ranit Kedmi^{1,2,3,4,5}, Srinivas Ramishetti^{1,2,3,4}, Nuphar Veiga^{1,2,3,4}, Ashley M. Jacobi⁶, Mollie S. Schubert⁶, Dinorah Friedmann-Morvinski⁷, Zvi R. Cohen⁸, Mark A. Behlke⁶, Judy Lieberman⁹, Dan Peer^{1,2,3,4†}

Harnessing CRISPR-Cas9 technology for cancer therapeutics has been hampered by low editing efficiency in tumors and potential toxicity of existing delivery systems. Here, we describe a safe and efficient lipid nanoparticle (LNP) for the delivery of Cas9 mRNA and sgRNAs that use a novel amino-ionizable lipid. A single intracerebral injection of CRISPR-LNPs against *PLK1* (sgPLK1-cLNPs) into aggressive orthotopic glioblastoma enabled up to ~70% gene editing in vivo, which caused tumor cell apoptosis, inhibited tumor growth by 50%, and improved survival by 30%. To reach disseminated tumors, cLNPs were also engineered for antibody-targeted delivery. Intraperitoneal injections of EGFR-targeted sgPLK1-cLNPs caused their selective uptake into disseminated ovarian tumors, enabled up to ~80% gene editing in vivo, inhibited tumor growth, and increased survival by 80%. The ability to disrupt gene expression in vivo in tumors opens new avenues for cancer treatment and research and potential applications for targeted gene editing of noncancerous tissues.

INTRODUCTION

In recent years, molecularly targeted inhibitors and immunotherapy have greatly improved cancer responses with reduced toxicity and adverse reactions. However, the high recurrence rate and the development of drug resistance for most types of cancers highlight the need for new therapeutic modalities. Most cancer drugs require repeated administration, which increases treatment-related toxicity and treatment cost and severely reduces patient quality of life. CRISPR-Cas9 gene editing has the potential to permanently disrupt tumor survival genes, which could overcome the repeated dosing limitations of traditional cancer therapies, improve treatment efficacy, and require fewer treatments (1, 2). The Cas9 nuclease is directed by a single-guide RNA (sgRNA) to modify a specific chromosomal DNA sequence by inducing a sequence-specific double-strand break (DSB) (3, 4). DSBs are predominantly resolved via the error-prone non-homologous end-joining repair mechanism, which can induce insertions or deletions that result in gene disruption. However, the large size of Cas9 (160 kDa, 4300 bases) and sgRNA (~31 kDa, 130 bases) is an obstacle for conventional viral and nonviral delivery systems. Moreover, current delivery systems for nonliver tissues and tumors only result in relatively low gene editing percentages (5, 6). For an effective cancer therapy, substantially higher editing efficiencies would be needed.

¹Laboratory of Precision Nanomedicine, The Shmunis School of Biomedicine and Cancer Research, George S. Wise Faculty of Life Sciences, Tel Aviv University, Tel-Aviv, Israel. ²Department of Materials Sciences and Engineering, Iby and Aladar Fleischman Faculty of Engineering, Tel Aviv University, Tel Aviv, Israel. ³Center for Nanoscience and Nanotechnology, Tel Aviv University, Tel Aviv, Israel. ⁴Cancer Biology Research Center, Tel Aviv University, Tel Aviv, Israel. ⁵Molecular Pathogenesis Program, The Kimmel Center for Biology and Medicine of the Skirball Institute, New York University School of Medicine, New York, NY 10016, USA. ⁶Integrated DNA Technologies Inc., Coralville, IA 52241, USA. ⁷Sagol School of Neuroscience, Department of Biochemistry and Molecular Biology, The George S. Wise Faculty of Life Sciences, Tel Aviv University, Tel Aviv, Israel. ⁸Department of Neurosurgery, Sheba Medical Center, Ramat-Gan, and Sackler School of Medicine, Tel Aviv University, Tel Aviv 6997801, Israel. ⁹Program in Cellular and Molecular Medicine, Boston Children's Hospital, and Department of Pediatrics, Harvard Medical School, Boston, MA 02115, USA.

*These authors contributed equally to this work.

†Corresponding author. Email: peer@tauex.tau.ac.il

Lipid nanoparticles (LNPs) are clinically approved nonviral nucleic acid delivery systems capable of delivering potentially such large payloads. Cationic ionizable lipids are the key component of LNPs that enables efficient nucleic acid encapsulation, cellular delivery, and endosomal release. However, LNP formulations that were optimized for small interfering RNA (siRNA) delivery do not efficiently deliver large nucleic acids (e.g., mRNAs and plasmids) (7, 8). Most in vivo studies of gene editing have relied on adeno-associated virus (AAV) to deliver CRISPR components locally to the retina or skeletal muscle or to the liver. Nevertheless, AAV applications are limited by its small carrying capacity, immune responses, hepatotoxicity at high doses, and the lack of cellular targeting (9, 10). Several nonviral delivery vehicles for CRISPR components have been reported in recent years (5, 11). These systems were evaluated for liver-associated genetic diseases, demonstrated gene editing of up to 60% in mice and rat livers, and almost a complete reduction of target protein in the blood. However, formulations designed for other tissues were less efficient (i.e., up to ~15% in the lung and ~3% in melanoma) (5, 6). Therefore, the development of efficient and safe delivery systems for nonliver tissues remains an important missing link for therapeutic translation of CRISPR editing.

Here, we report the development of a targeted nonviral LNP delivery system for therapeutic genome editing and evaluate it in two aggressive and incurable cancer models.

RESULTS

Development and characterization of LNPs encapsulating Cas9 mRNA and sgRNA

To overcome the cargo limitation of currently available LNP formulations, LNPs were designed to coencapsulate Cas9 mRNA and sgRNA, using ionizable cationic lipids from a novel ionizable amino lipid library (Fig. 1A) (12). This library was constructed using a novel class of ionizable amino lipids based on hydrazine, hydroxylamine, and ethanolamine linkers with a linoleic fatty acid chain and amine head groups (12). Lipids 1, 6, 8, and 10 were the top hits of the screen and were chosen for further evaluation for CRISPR-Cas9

Copyright © 2020
The Authors, some
rights reserved;
exclusive licensee
American Association
for the Advancement
of Science. No claim to
original U.S. Government
Works. Distributed
under a Creative
Commons Attribution
NonCommercial
License 4.0 (CC BY-NC).

Downloaded from https://www.science.org at Science and Technology Facilities Council on January 19, 2024

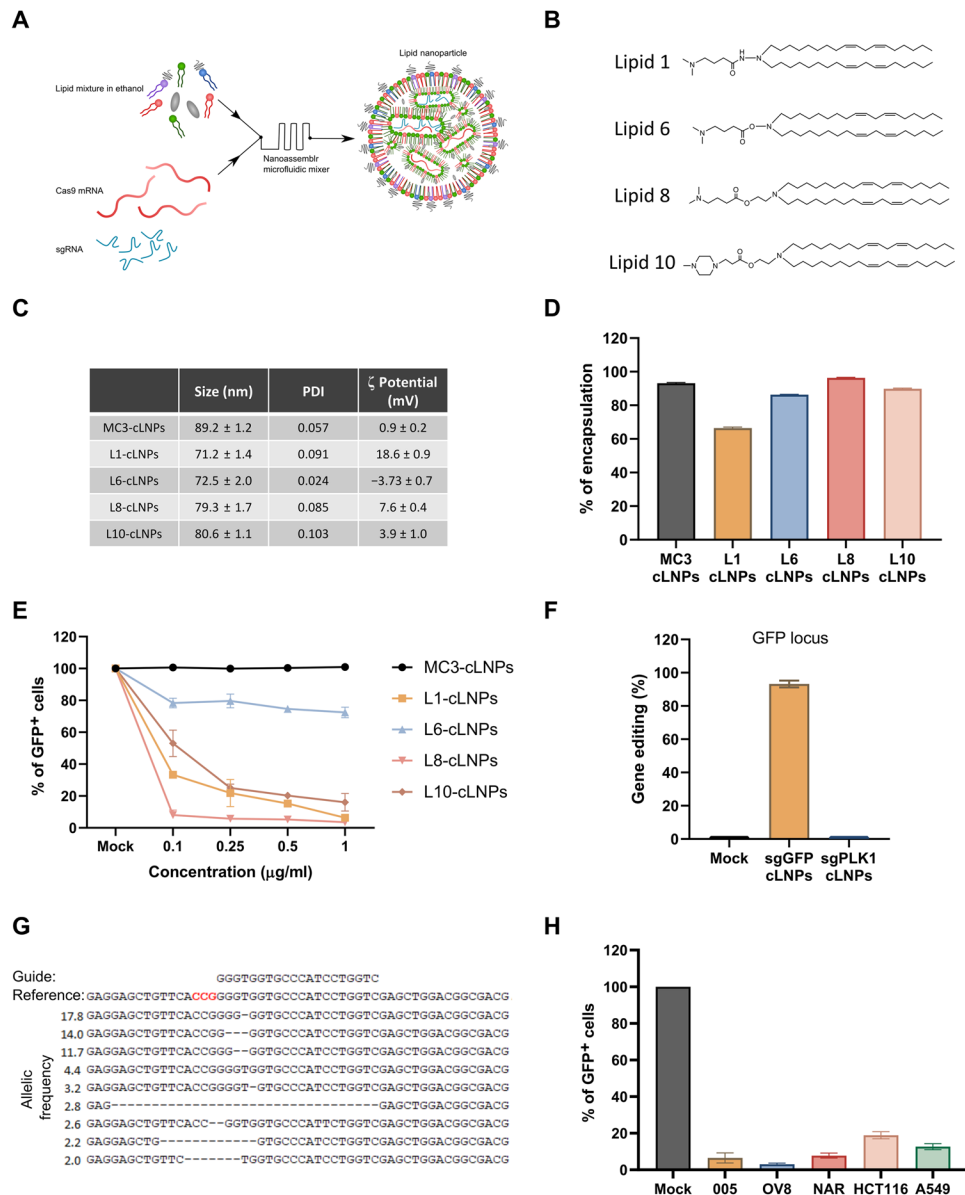


Fig. 1. Design and construction of CRISPR LNPs (cLNPs). (A) Schematic illustration of cLNP preparation. A microfluidic-based mixing of lipids to construct cLNPs encapsulating Cas9 mRNA and sgRNA. (B) Chemical structures of the selected ionizable amino lipids from the library screen. (C) Physicochemical characterization of cLNP by dynamic light scattering and ζ sizer. Data are means ± SD of five independent preparations. (D) Encapsulation efficiency as measured using a RiboGreen assay. (E) GFP disruption assay: HEK293 cells were transfected with cLNPs at different concentrations (0.1 to 1 μg/ml, 0.7 to 7 nM total RNA), and 72 hours after transfection, the percentage of GFP⁺ cells were analyzed by flow cytometry. Data are means ± SD of three independent experiments. (F and G) Percentage of gene editing events upon either GFP or PLK1-cLNP transfection (F) in the GFP loci as determined by NGS analysis (allelic frequencies of >2% are presented). (H) GFP disruption assay in multiple cancer cell lines compared to mock-treated cells. Cells were transfected with L8-cLNPs, and 72 hours after transfection, the percentage of GFP⁺ cells were analyzed by flow cytometry. Data are means ± SD of three independent experiments.

gene editing (Fig. 1B). Cas9 mRNA was chosen, instead of plasmid DNA, to reduce long-term exposure to the nuclease to minimize off-target gene modifications (13, 14). To enhance RNA stability and minimize immunogenicity, Cas9 mRNA was chemically modified with 5-methoxyuridine, and highly modified sgRNAs were used (IDT sgRNA XT) (15, 16). CRISPR-LNP (cLNP) formulations containing Cas9 mRNA and an sgRNA were compared to Cas9 mRNA and sgRNAs encapsulated with the clinically approved LNP formulation, used for siRNA therapeutics, based on DLin-MC3-DMA as the ion-

izable cationic lipid (MC3-cLNPs). cLNPs were uniform in size with a diameter of 71 to 80 nm, polydispersity index of 0.024 to 0.103, and ζ potential of -3 to 18.6 mV as measured by dynamic light scattering (Fig. 1C). The biophysical properties and transmission electron microscopy micrographs of L8-cLNPs were similar to those of MC3-cLNPs (Fig. 1C and fig. S1A). The encapsulation efficiency of Cas9 mRNA and sgRNA in L6, L8, L10, and MC3-LNPs was similarly high (>90%) but lower in L1-cLNPs (~65%) (Fig. 1D). Next, we evaluated the in vitro gene disruption efficiency of the cLNP formulations

encapsulating a *GFP* sgRNA by measuring the loss of green fluorescent protein (GFP) fluorescence in human embryonic kidney (HEK) 293 cells stably expressing GFP (HEK293/GFP) (Fig. 1E) (17). L1-, L8-, and L10-cLNPs all disrupted *GFP* in a concentration-dependent manner, and L8 was the most efficient. GFP fluorescence was detected in only 4% of L8-cLNP-treated cells after incubation with cLNPs containing total RNA (1.0 $\mu\text{g}/\text{ml}$). Although Cy5.5-labeled MC3-cLNPs were taken up more efficiently than L8-cLNPs into HEK293/GFP cells as measured by flow cytometry (fig. S1B), MC3-cLNPs did not reduce GFP expression at any concentration (0.1 to 1.0 $\mu\text{g}/\text{ml}$ total RNA, 0.7 to 7 nM total RNA). On the basis of these data, L8-cLNPs were chosen for further study.

The efficiency and specificity of gene disruption by L8-cLNPs encapsulating *GFP* sgRNAs (sgGFP-cLNPs) in HEK293/GFP were assessed by quantifying the percent of gene-edited *GFP* genomic sequences by next-generation sequencing (NGS). Ninety-four percent of *GFP* genomic DNA was modified, but <0.1% was edited at a non-targeted locus (*PLK1*) (Fig. 1, F and G). sgGFP-cLNPs did not significantly affect cell viability at all tested concentrations (up to 1 $\mu\text{g}/\text{ml}$; fig. S2). Next, we evaluated gene disruption using L8-cLNPs in multiple GFP-expressing, aggressive cancer cell lines [005 murine glioblastoma multiforme (GBM), human serous ovarian adenocarcinomas Ovar8 (OV8) and NCI-ADR (NAR), human colon carcinoma HCT116, and human lung adenocarcinoma A549]. After incubation with sgGFP-cLNPs (1 $\mu\text{g}/\text{ml}$; 7 nM of total RNA), GFP fluorescence was only detected in 3 to 18% of these cancer cells (Fig. 1H). Thus, L8-cLNPs cause efficient and specific gene editing in vitro with low toxicity in multiple cancer cell lines.

sgPLK1-cLNPs induce efficient therapeutic gene editing, cell cycle arrest, and cell death in vitro

To explore the potential of therapeutic genome editing, as proof of concept, we evaluated L8-cLNPs containing *PLK1* sgRNA (sgPLK1-cLNPs) or sgGFP-cLNPs as control. *PLK1* is a kinase required for mitosis; lack of it leads to G₂-M phase cell cycle arrest and cell death in dividing cells. Treating HEK293/GFP with sgPLK1-cLNPs (0.5 $\mu\text{g}/\text{ml}$) caused 98% *PLK1* gene editing, while <0.1% was edited at the non-targeted *GFP* locus by NGS (Fig. 2, A and B). *PLK1* gene editing caused potent G₂-M arrest 48 hours later, while control sgGFP-cLNPs had no effect on cell cycle profile (Fig. 2, C and D). Treatment with sgPLK1-cLNP resulted in a fivefold decrease in cell viability compared to untreated or sgGFP-cLNP-treated cultures, as analyzed by 4',6-diamidino-2-phenylindole (DAPI)/annexin V staining and by XTT assay, 96 hours after treatment (Fig. 2, E to G). Preserved cell viability after treatment with sgGFP-cLNPs suggests that cLNPs may have low toxicity at therapeutically relevant doses.

sgPLK1-cLNP gene editing induces cell cycle arrest and cell death of cancer cell lines in vitro

To explore the potential of cLNPs for therapeutic genome editing in cancer, we evaluated cancer cell lines of two aggressive and difficult to treat cancers—the murine GBM stem cell-like 005 cell line isolated from gliomas that formed in *Tp53*^{+/-} mice after intracerebral lentiviral transduction of activated H-Ras and Akt (18, 19) and human OV8, a high-grade serous ovarian adenocarcinoma cell line that is highly drug resistant and metastasizes to form ascites (20, 21). GBM 005 cells resemble almost uniformly fatal human GBM, in that they are highly invasive, neovascularized, pleomorphic, and infiltrated by immune cells (18, 19). Intraperitoneally injected OV8 form chemo-

resistant, metastatic, high-grade ovarian cancer xenografts, like most human ovarian cancers. In vitro incubation of GBM 005 or OV8 with sgPLK1, but not sgGFP, cLNPs efficiently disrupted the *PLK1* gene, causing 84 and 91% genomic editing, respectively (Fig. 3, A and F, and fig. S3). Disruption of *PLK1* also strongly caused G₂-M cell cycle arrest 48 hours after treatment (Fig. 3, B, C, G, and H, and fig. S4, A and C) and reduced cell viability 96 hours after treatment by 5-fold in GBM 005 and 10-fold in OV8, respectively (Fig. 3, D and I). Similarly, DAPI and/or annexin V staining increased after incubation with sgPLK1, but not sgGFP-cLNPs (Fig. 3, E and J, and fig. S4, B and D). Thus, sgPLK1-cLNPs efficiently disrupted the targeted gene and caused cell cycle arrest and death of GBM 005 and OV8 in vitro.

cLNPs are safe and nonimmunogenic after systemic administration

To evaluate the therapeutic potential of cLNPs for cancer, we needed to address two major concerns about CRISPR-Cas9 therapeutics: potential toxicity and immunogenicity. An initial study evaluated liver toxicity, blood counts, and serum inflammatory cytokines 24 hours after intravenous injection of sgGFP-cLNPs (1 mg/kg) into C57BL/6 mice. There were no apparent clinical signs of toxicity and no significant difference in liver enzyme (alanine transaminase, aspartate aminotransferase, and alkaline phosphatase) levels (fig. S5A) or blood counts (fig. S5B). A plasma cytokine panel [interleukin-1 β (IL-1 β), IL-2, tumor necrosis factor- α (TNF- α), interferon- γ (IFN- γ), and IL-10] also showed no significant differences (fig. S5C). Although more extensive evaluation of potential toxicity is needed for preclinical development, these results suggest that L8-cLNPs are not toxic or immunogenic when administered systemically at therapeutically relevant doses (see below).

A single administration of sgPLK1-cLNPs potently inhibits tumor growth and increases survival in orthotopic GBM

Next, we evaluated whether the high genome editing efficacy observed in vitro could be translated to therapeutic efficacy in vivo. GBM 005 cells expressing GFP, mCherry, and luciferase were injected stereotactically into the mouse hippocampus. (Fig. 4A). Ten days later, Cy5.5-labeled sgGFP-cLNPs or phosphate-buffered saline (PBS) was injected intratumorally, and mice were euthanized 6 hours later to evaluate the tumor distribution by fluorescence microscopy. The Cy5.5-labeled cLNPs distributed throughout the tumor (Fig. 4B). To evaluate in vivo gene editing, sgGFP-cLNPs (0.05 mg/kg) were injected stereotactically into established tumors, mice were euthanized 2 days later, and single-cell tumor suspensions were analyzed by NGS for GFP gene editing. A single intracerebral injection facilitated ~72% of editing in the GFP locus in tumor cells (fig. S6A). To validate whether gene editing will translate to a loss of GFP fluorescence, sgGFP-cLNPs (0.05 mg/kg) were injected stereotactically into established tumors, mice were euthanized 7 days later, and single-cell tumor suspensions were analyzed by flow cytometry for GFP expression. GFP fluorescence in tumor cells was reduced by about twofold, demonstrating in vivo gene disruption (fig. S6, B and C). Next, to evaluate *PLK1* gene disruption in vivo, either sgPLK1 or sgGFP-cLNPs (0.05 mg/kg) were injected stereotactically into established tumors, mice were euthanized 2 days later, and single-cell tumor suspensions were analyzed by NGS for *PLK1* gene editing. sgPLK1-cLNPs facilitated ~68% editing in the *PLK1* locus in tumor cells (Fig. 4C). To evaluate in vivo apoptosis caused by *PLK1* gene

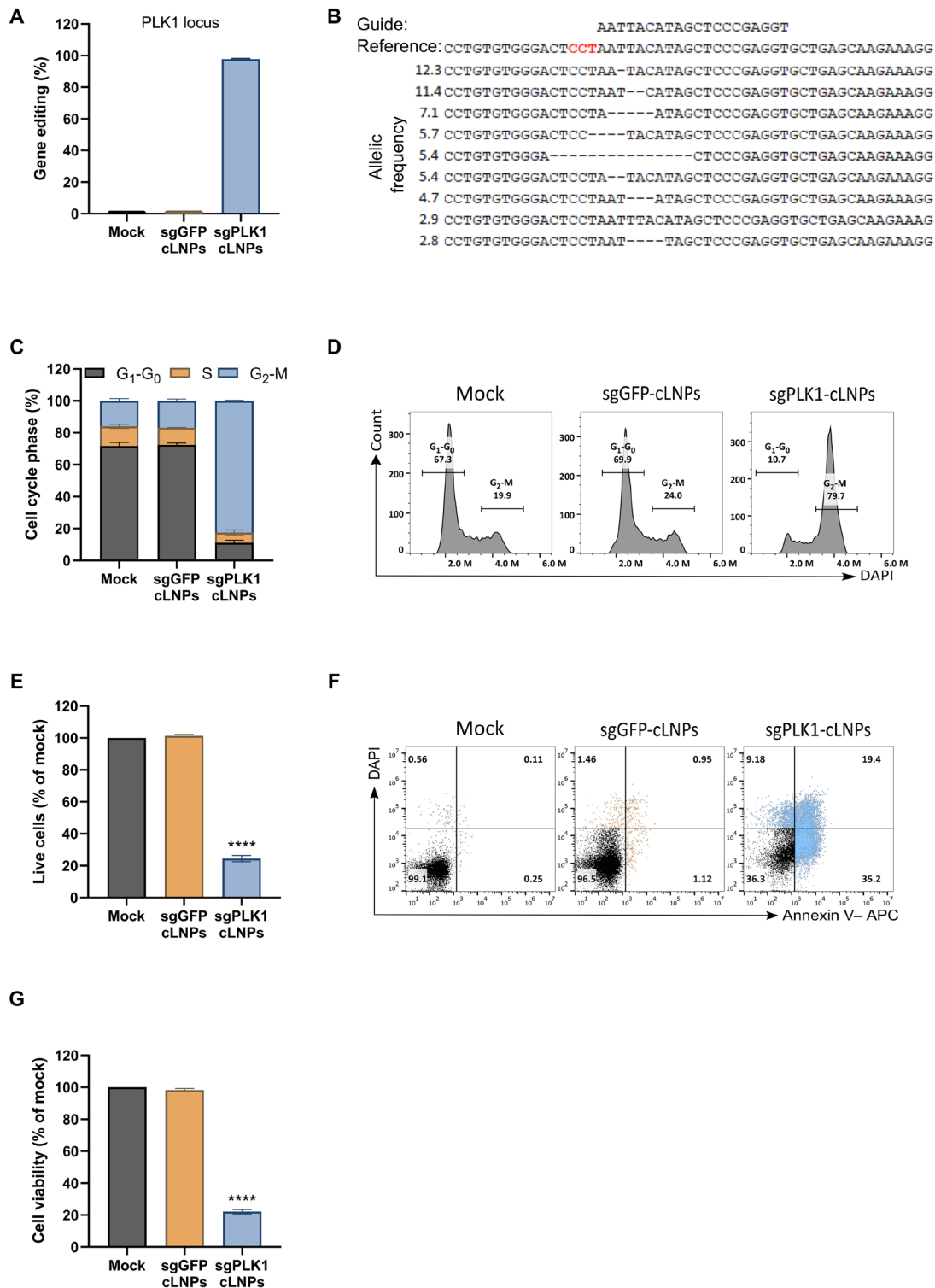


Fig. 2. Therapeutic genome editing in HEK293 cells in vitro. (A and B) Percentage of gene editing events (A) and allelic frequencies (B) in the PLK1 loci as determined by NGS analysis (allelic frequencies of >2% are presented). (C and D) Cell cycle analysis of HEK293 cells treated with mock, sgGFP, or sgPLK1-cLNPs (0.5 μg/ml, 3.5 nM of total RNA) for 48 hours and analyzed by flow cytometry. (C) Bar charts representing the percentage of G₁-S and G₂-M cell cycle phases. Data are means ± SD of three independent experiments. (D) Representative cell cycle analysis diagram. (E and F) DAPI/annexin V assay of HEK293 cells treated with mock, sgGFP, or sgPLK1-cLNPs (0.5 μg/ml, 3.5 nM total RNA) for 96 hours and analyzed by flow cytometry. (E) Bar charts representing the percentage of live cells normalized to mock-treated cells. Data are means ± SD of three independent experiments. (F) Representative DAPI/annexin assay diagram. (G) XTT cell viability assay of HEK293 cells treated with mock, sgGFP, or sgPLK1-cLNPs (0.5 μg/ml, 3.5 nM total RNA) 96 hours after treatment. Bar charts representing the % of cell viability normalized to mock-treated cells. Data are means ± SD of three independent experiments. (E and G) One-way analysis of variance (ANOVA) with Tukey multiple comparison test was used to assess the significance. *****P* < 0.0001.

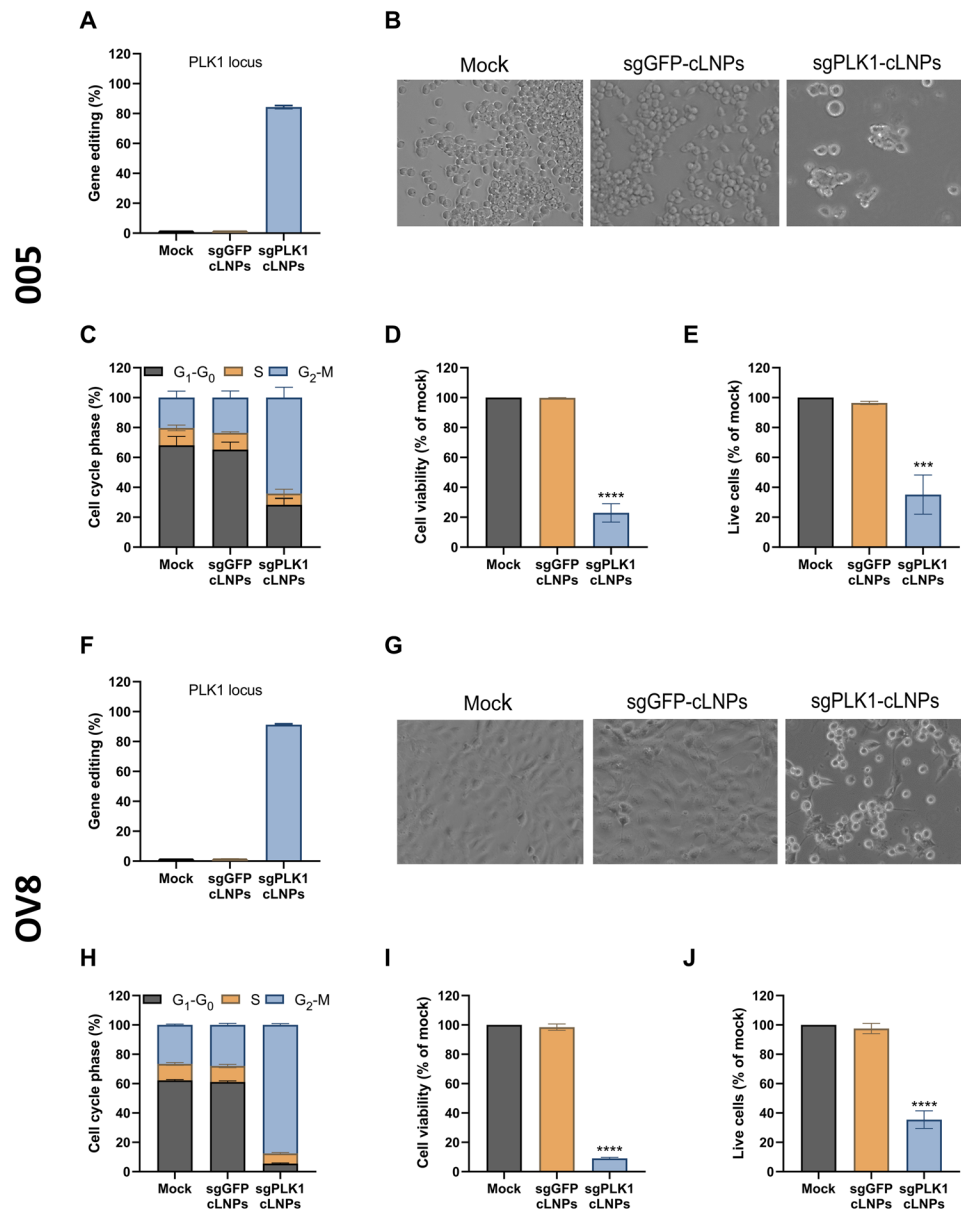


Fig. 3. Therapeutic genome editing in 005 (murine GBM) and OV8 (human ovarian carcinoma) cells in vitro. (A and F) Percentage of gene editing events in the PLK1 loci in 005 and OV8 as determined by NGS analysis. (B and G) Bright-field microscopy representative images of 005 and OV8 cells treated with mock, sgGFP, or sgPLK1-cLNPs [005: 0.5 $\mu\text{g}/\text{ml}$ (3.5 nM total RNA); OV8: 1 $\mu\text{g}/\text{ml}$ (7 nM total RNA)], 72 hours after treatment. (C and H) Cell cycle analysis of 005 and OV8 cells, treated with mock, sgGFP, or sgPLK1-cLNPs [005: 0.5 $\mu\text{g}/\text{ml}$ (3.5 nM total RNA); OV8: 1 $\mu\text{g}/\text{ml}$ (7 nM total RNA)] for 48 hours and analyzed by flow cytometry. Bar charts representing the % of G₁, S, and G₂-M cell cycle phases. Data are means \pm SD of three independent experiments. (D and I) XTT cell viability assay of 005 and OV8 cells treated with mock, sgGFP, or sgPLK1-cLNPs [005: 0.5 $\mu\text{g}/\text{ml}$ (3.5 nM total RNA), OV8: 1 $\mu\text{g}/\text{ml}$ (7 nM total RNA)] for 96 hours. Bar charts representing the % of cell viability normalized to mock-treated cells. Data are means \pm SD of three independent experiments. (E and J) DAPI/annexin V apoptosis analysis of 005 or OV8 cells treated with mock, sgGFP, or sgPLK1-cLNPs [005: 0.5 $\mu\text{g}/\text{ml}$ (3.5 nM total RNA); OV8: 1 $\mu\text{g}/\text{ml}$ (7 nM total RNA)] for 96 hours and analyzed by flow cytometry. Bar charts representing the percentage of live cells normalized to mock-treated cells. Data are means \pm SD of three independent experiments. (C, E, and H to J) One-way ANOVA with Tukey multiple comparison test was used to assess the significance. **** P < 0.0001 and *** P < 0.001.

disruption, either sgPLK1 or sgGFP-cLNPs (0.05 mg/kg) were injected stereotactically into established tumors. Mice were euthanized 3 days later, and tumor sections were analyzed by fluorescence microscopy for caspase-3 activation. Activated caspase-3 was only present in sgPLK1-cLNP-treated tumors, while no apparent staining was visualized in tumors treated with sgGFP-cLNPs, demonstrating *PLK1*-dependent apoptosis (Fig. 4D). Adjacent normal GFP tissue also did

not show any evidence of caspase-3 activation. Because neurons are terminally differentiated nondividing cells, normal brain tissue has minimal expression of *PLK1*; therefore, it is not expected to undergo apoptosis. Next, we evaluated whether sgPLK1-cLNPs can inhibit tumor growth. GBM 005-bearing mice were injected stereotactically once with sgPLK1 or sgGFP-cLNPs (0.05 mg/kg) (Fig. 4E). A single intratumoral injection of sgPLK1-cLNPs significantly reduced tumor

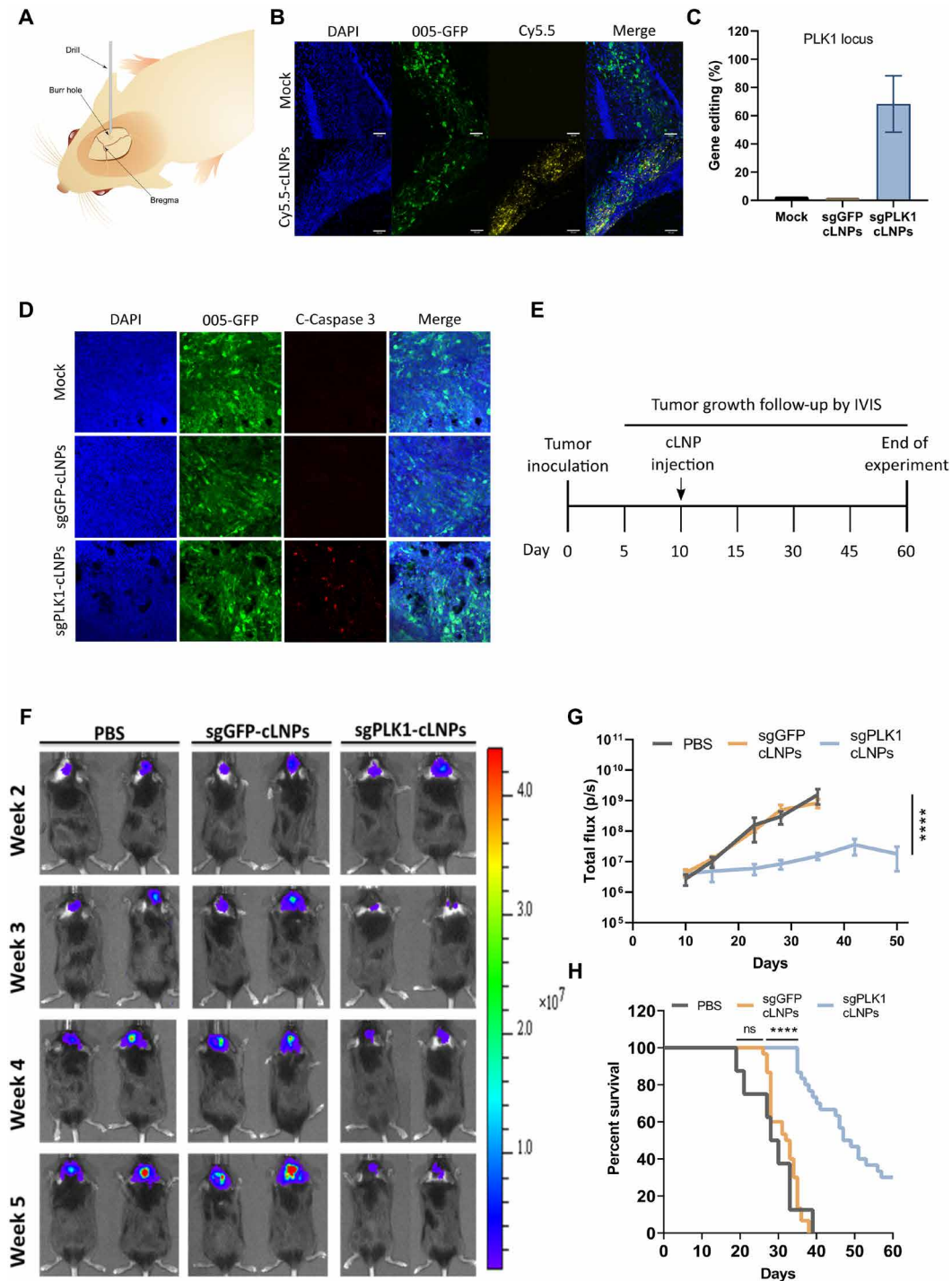


Fig. 4. Therapeutic genome editing in 005 GBM bearing mice. (A) Schematic illustration of intracerebral injection to mouse brain. (B) cLNP dispersion through the tumor lesion upon intracerebral injection of Cy5.5-cLNPs to the tumor bed of 005 GBM-bearing mice. Brain sections were analyzed by confocal microscopy, 6 hours after injection. Blue, DAPI; green, 005 GFP cells; yellow, Cy5.5 cLNPs. Scale bars, 50 μ m. (C) Percentage of gene editing events in the PLK1 locus as determined by NGS analysis, 48 hours after injection of PBS or 0.05 mg/kg of sgGFP-cLNPs or sgPLK1-cLNPs. (D) In vivo apoptosis induction using activated caspase 3 staining upon injection of either PBS or 0.05 mg/kg of sgGFP-cLNPs or sgPLK1-cLNPs. Brain sections were analyzed by confocal microscopy 3 days after injection. Blue, DAPI; green, 005 GFP cells; red, cleaved caspase 3. Scale bars, 50 μ m. (E) Experimental design. Ten days after tumor inoculation, sgGFP-cLNPs, sgPLK1-cLNPs, or PBS (0.05 mg/kg) was injected into the tumor bed. Tumor growth was monitored using bioluminescence of 005-GFP-Luc cells by the IVIS in vivo imaging system. (F and G) Tumor growth inhibition by single-dose treatment with cLNPs. (F) Representative bioluminescence imaging of 005 GBM-bearing mice. (G) 005 tumor growth curve quantification. Data are presented in total flux (p/s) \pm SEM; $n = 15$ animals per treatment group and $n = 8$ animals in the PBS group, **** $P < 0.0001$. One-way ANOVA was used to assess the significance at day 41. (H) Survival curves of 005 GBM-bearing mice. $n = 30$ animals per treatment group and $n = 8$ animals in the PBS group. **** $P < 0.0001$. Log-rank (Mantel-Cox) test was used for curve comparison.

growth compared to control groups as quantified by live animal luciferase activity (Fig. 4, F and G) and increased median survival from 32.5 to >48 days (Fig. 4H). Thirty percent of sgPLK1-cLNP-treated mice survived for 60 days when the experiment was terminated, while all the control mice died by 40 days. sgGFP-cLNPs had no significant effect on tumor growth or survival. As far as we are aware, these findings represent the highest survival improvement in this aggressive tumor after a single treatment.

EGFR-targeted sgPLK1-cLNPs potently inhibit tumor growth and increase overall survival in metastatic ovarian adenocarcinoma model

Therapeutic strategies for most tumors, especially metastatic or hematological tumors, require systemic rather than local administration. However, most LNPs get trapped in the liver and other central organs and are not efficiently taken up by tumor cells after systemic injection. A strategy for cell-targeted gene editing could enhance gene editing of tumor cells and reduce toxicity and editing of non-transformed cells. We recently reported a flexible method for antibody-targeted cell-specific delivery of siRNAs and mRNAs using systemically injected LNPs (22, 23). These targeted LNPs are coated with cell-targeting antibodies by binding to a lipid-anchored single-chain antibody linker that recognizes the Fc region of rat immunoglobulin G2a [IgG2A; Anchored Secondary scFv Enabling Targeting (ASSET)] (Fig. 5A) and reduce the recognition of the targeting antibody by Fc receptors (23). To evaluate the in vivo therapeutic potential of targeted L8-cLNPs (T-cLNP) against human OV8 peritoneal xenografts, we used the fact that these tumors highly express the epidermal growth factor receptor (EGFR) (24) to target cLNPs to OV8 by coating them with anti-EGFR. Mice bearing disseminated peritoneal OV8-mCherry tumors were injected intraperitoneally 10 days after tumor inoculation with Cy5.5-labeled sgGFP-cLNPs (0.75 mg/kg) conjugated to anti-hEGFR (T) or IgG isotype control (I) antibody (T- or I-Cy5.5-cLNPs, respectively) to explore tumor targeting and accumulation. Four hours later, tumors were collected, and the Cy5.5 signal in the tumors was measured by live animal fluorescent imaging. Cy5.5 signal in the tumor was three times higher in T-Cy5.5-cLNP-treated mice rather than in I-Cy5.5-cLNP-treated mice, demonstrating specific targeting and accumulation in the tumor of T-cLNPs (Fig. 5, B and C). Next, to evaluate in vivo *PLK1* gene disruption, mice bearing metastatic OV8-mCherry tumors were injected intraperitoneally 10 days after tumor inoculation with sgPLK1 or sgGFP-cLNPs (0.75 mg/kg) conjugated to anti-hEGFR (T) or IgG isotype control (I) antibody (T- or I-cLNPs). Mice were euthanized 2 days later, tumors were collected, and single-cell tumor suspensions were analyzed by NGS for *PLK1* gene editing. T-sgPLK1-cLNPs facilitated ~82% of editing in the *PLK1* locus in tumor cells, but <1% was detected in control groups (Fig. 5D). To evaluate anti-tumor effectiveness, mice bearing metastatic OV8-mCherry tumors were injected intraperitoneally on days 10 and 17 after tumor inoculation with either T-sgPLK1-cLNPs, I-sgPLK1-cLNPs, T-sgGFP-cLNPs, or I-sgGFP-cLNPs (0.75 mg/kg) (Fig. 5E). Tumor growth, monitored using mCherry live animal fluorescent imaging, was strongly inhibited only by T-sgPLK1-cLNPs (Fig. 5, F and G) and increased overall survival by ~80% (Fig. 5H). No significant difference in tumor growth or survival was observed in control mice treated with either T-sgGFP-cLNPs, I-sgGFP-cLNPs, or I-sgPLK1-cLNPs (Fig. 5G). These findings suggest that targeted cLNPs may be useful for targeted treatment of disseminated tumors.

DISCUSSION

Remarkable progress has been made to improve the efficacy and safety of CRISPR-Cas9 gene editing (4, 25–28). However, broad clinical translation will be enhanced by safe delivery systems able to edit efficiently specific diseased tissues in vivo (3, 29–31). Because of the large size of the Cas9 nuclease, its encapsulation in both viral and nonviral delivery systems remains a challenge. Several approaches have been used to overcome the obstacle of delivering the large Cas9 nuclease as nucleic acid or protein for gene editing in the liver or locally for treating genetic disorders (5, 32–35). These approaches achieved about 60% gene editing in the liver, resulting in reduced protein or cholesterol levels in the serum and alleviating disease symptoms in models of hemophilia, hypercholesterolemia, or TTR (transthyretin) amyloidosis (5, 11, 36). To date, systemic administration results in low editing efficiencies in extrahepatic tissues, partly due to the lack of specific targeting of current delivery vehicles. To achieve therapeutic effects for nonliver diseases or disseminated diseases, such as cancer, higher tissue-specific targeting with sufficient editing efficiencies is needed. Other genetic therapies, such as those based on RNA interference (RNAi), are transient and, therefore, would require repeated dosing, especially for rapidly dividing cancer cells. The permanent nature of genome editing should have a therapeutic impact even after one or a few doses, which could strongly affect toxicity, development of adverse reactions, compliance, and cost. Furthermore, the bacterial origin of the Cas9 nuclease renders it to be recognized by the host immune system and elicits an immune response (37, 38). Long exposure time to the Cas9 nuclease, as well as repeating dosing, might increase the risk for Cas9-related immune responses following by immune-related adverse reactions and treatment failure. Therefore, to minimize this risk, delivery systems that could achieve therapeutic relevant genome editing with a limited number of administrations and short Cas9 exposure time must be developed.

In this study, we developed and tested an efficient nonviral LNP system for CRISPR-Cas9 gene editing, which showed gene editing of up to 98% in vitro in multiple cancer cell types and up to ~80% gene editing in vivo. cLNPs targeting *PLK1* were able to inhibit tumor growth and improve survival in two aggressive cancer models in mice following single or double cLNP administrations. A single dose of sgPLK1-cLNPs to the tumor bed of a murine GBM model resulted in ~70% gene editing of the *PLK1* gene, induced in vivo apoptosis as assessed by activated caspase 3 staining, prolonged median survival by ~50%, and improved overall survival of 005 GBM-bearing mice by 30%. The blood-brain barrier (BBB) is a highly restrictive barrier for most therapeutic modalities. The clinical course of this devastating disease has not changed for over a decade, partly due to the limitation presented by the low BBB permeability to standard chemo- and immunotherapies. In recent years, multiple clinical trials have been conducted using local intracerebral administration with or without tumor resection to bypass the BBB; however, the success of these clinical trials was hampered by the low diffusion of the tested drugs and severe damages to the healthy brain parenchyma (39–41). Our results highlight the potential of cLNPs to overcome the limitations of current therapies in a clinically relevant tumor model.

To reach disseminated tumors, we also constructed cell-targeted cLNPs, decorated with an antibody to an overexpressed receptor on ovarian cancer cells. EGFR-targeted cLNPs accumulated in disseminated tumors significantly more than IgG control cLNPs, demonstrating the advantage of a cell-targeted approach for disseminated tumors. Furthermore, a single administration of EGFR-targeted

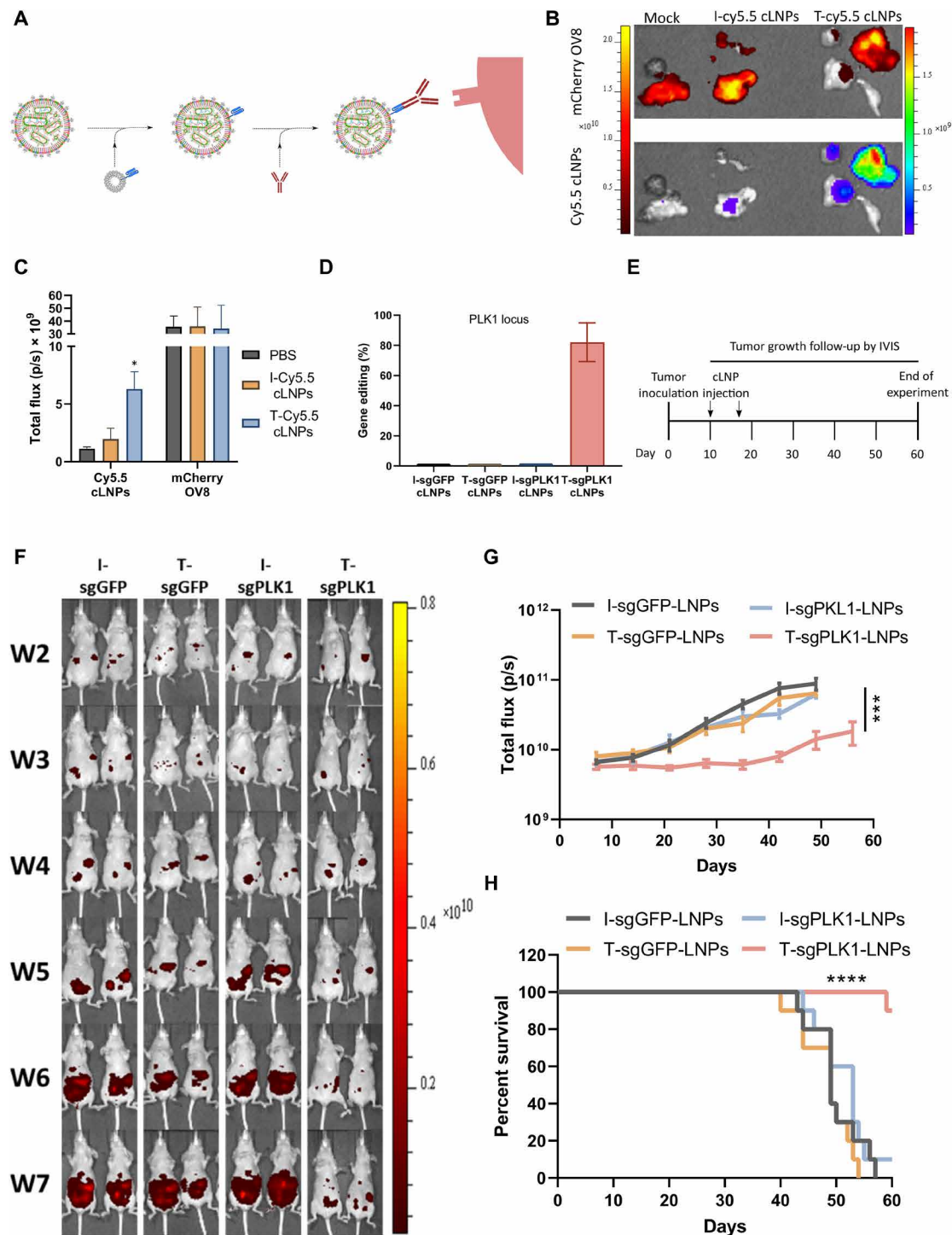


Fig. 5. Therapeutic genome editing in OV8-bearing mice. (A) Schematic illustration of targeted cLNP production using ASSET (23). (B and C) Tumor targeting and accumulation of Cy5.5-cLNPs in OV8 tumor-bearing mice as analyzed by the IVIS in vivo imaging system, 4 hours after injection. (B) Representative fluorescence imaging of tumors extracted from mCherry-OV8-bearing mice. Top, mCherry OV8 tumors; bottom, Cy5.5-cLNP signal accumulation. (C) Quantification of mean fluorescence intensity of Cy5.5-cLNP accumulation in mCherry-OV8 tumors. Data are means \pm SD of three independent experiments. One-way ANOVA was used to assess the significance, $*P < 0.05$. (D) Percentage of gene editing events in the PLK1 locus as determined by NGS analysis, 48 hours after injection of I-sgGFP, T-sgGFP, I-sgPLK1, or T-sgPLK1 cLNPs (0.75 mg/kg). (E) Experimental design. Ten and 17 days after tumor inoculation, I-sgGFP, T-sgGFP, I-sgPLK1, or T-sgPLK1 cLNPs (0.75 mg/kg) were injected intraperitoneally. Tumor growth was monitored using mCherry fluorescence of OV8-mCherry cells by the IVIS in vivo imaging system. (F and G) Tumor growth inhibition by dual-dose treatment with cLNPs. (F) Representative fluorescence imaging of OV8-bearing mice. (G) OV8 tumor growth curve quantification. Data are presented in total flux (p/s) \pm SEM; $n = 10$ per group. One-way ANOVA was used to assess the significance at day 49; $****P < 0.0001$. (H) Survival curves of OV8-bearing mice. $n = 10$ animals per treatment group. $****P < 0.0001$. Log-rank (Mantel-Cox) test was used for curve comparison.

cLNPs facilitated up to ~80% PLK1 gene editing *in vivo*. Two intraperitoneal injections of EGFR-targeted sgPLK1-cLNPs greatly reduce tumor growth and increased overall survival by ~80% of mice with high-grade ovarian cancer malignant ascites. The majority of ovarian cancers are diagnosed at late stages when tumor metastasizes throughout the peritoneal cavity (42, 43). Recent clinical studies have demonstrated an improved pharmacokinetic profile of intraperitoneally injected chemotherapy resulting in higher drug concentration in the abdominal cavity and improved progression-free survival and overall survival. Furthermore, the partial systemic restriction of intraperitoneal administration resulted in reduced toxicity and treatment-related complications (44–46). The targeting strategy we designed, using the ASSET linker system (22, 23), is, to our knowledge, the first example of targeted CRISPR-Cas9 therapeutic gene editing for treating metastatic tumors. It provides a highly flexible and efficient strategy for targeted gene editing that could be used by changing the antibody, for targeting either tumor cells via tumor-specific cell surface receptors (such as EpCAM or PSMA) or shared tumor and normal cell receptors (such as CD19 on B cell lymphomas), or for targeting non-transformed cells in diseased tissues. Targeting provides a way of overcoming the limitations of most LNP and nanoparticle delivery systems, whose therapeutic effect is largely limited to the liver and other central organs, where particles get trapped. Moreover, targeted LNPs can be administered systemically to target both localized and disseminated (such as metastatic and/or hematopoietic) cells (22, 23).

In this study, we edited *PLK1* as proof of concept, but this cancer therapeutic strategy could be extended to edit tumor dependency genes that are not vital for normal tissues and to edit specific tumor dependency genes (such as BCR-ABL) or patient- and tumor-specific oncogene mutations (such as RAS). The Cas9 isolated from *Streptococcus pyogenes* was used for this proof-of-concept study but could be substituted with other CRISPR-associated nucleases to favor homologous recombination (HR) events or reduce off-target gene editing. Additional safety concern of translating CRISPR technologies to the clinic resides in off-target gene editing of bystander cells. This risk can be mitigated by the addition of tissue- or cell-specific miR binding sites to the mRNA sequence, which results in tissue-specific suppression of mRNA translation (47, 48). The main off-target site of LNP-based platforms is the liver, more specifically hepatocytes and Kupffer cells (49, 50), and suppression of mRNAs in these cell types can be achieved by inserting miR122 and miR142 binding sites, respectively. Using these tissue-specific mRNA suppression approaches is crucial for further clinical development of gene editing technologies. For noncancer applications, we could envision using targeted cLNPs for patient-tailored applications to correct genes associated with genetic deficiencies. Another application would be to disrupt a nonessential gene, whose knockout has no deleterious consequences but whose expression contributes to disease pathogenesis. One example is *CCR5*, whose knockout could potentially be used to prevent HIV transmission and cure HIV. Thus, this therapeutic strategy opens new avenues for using genome editing as a novel modality for treating various diseases and bringing CRISPR-Cas9 editing technology to the clinic.

METHODS

Cell lines

HEK293 [American Type Culture Collection (ATCC) CRL-1573], HCT116 (ATCC CCL-247), and A549 (ATCC CCL-185) cells were purchased from ATCC, and OV8 and NCI/ADR-RES (NAR) were

supplied by R. Margalit and maintained in Dulbecco's modified Eagle's medium (DMEM) or RPMI 1640 (Gibco, Thermo Fisher Scientific Inc.) supplemented with 10% fetal bovine serum (Biological Industries, Israel), 1% L-glutamine (Gibco, Thermo Fisher Scientific Inc.), and 1% penicillin-streptomycin-nystatin (Biological Industries, Israel). The 005 cells (supplied by D. Friedman-Morvinski) were maintained in stem cell medium, as previously described (15). GFP-expressing cells (HEK293 and NAR) were stably transfected with pQCXIP-GFP/d2. All cells were routinely checked every 2 months for mycoplasma contamination using the EZ-PCR Mycoplasma Test Kit (Biological Industries, Israel).

LNP preparation

DLin-MC3-DMA (MC3) and Lipid 8 were synthesized according to a previously described method (12, 23). Cholesterol, DSPC (1,2-distearoyl-sn-glycero-3-phosphocholine), polyethylene glycol (PEG)-DMG (1,2-dimyristoyl-rac-glycerol), and DSPE (1,2-distearoyl-sn-glycero-3-phosphoethanolamine)-PEG were purchased from Avanti Polar Lipids Inc. Briefly, one volume of lipid mixture (ionizable lipid, DSPC, cholesterol, DMG-PEG, and DSPE-PEG at 50:10.5:38:1.4:0.1 molar ratio) in ethanol and three volumes of mCas9/sgRNA (mCas9:sgRNA 3:1 weight ratio, 1:10 molar ratio RNA to ionizable lipid) in a citrate buffer were injected into a NanoAssemblr microfluidic mixing device (Precision Nanosystems Inc.) at a combined flow rate of 12 ml min⁻¹. The formed LNPs were dialyzed twice against PBS (pH 7.4) for 16 hours to remove ethanol.

Size distribution

cLNP size distribution and ζ potential were determined by dynamic light scattering using a Malvern Nano ZS ζ sizer (Malvern Instruments). For size measurements, cLNPs were diluted 1:20 in PBS. All used samples showed a PDI (polydispersity index) lower than 0.2. For ζ potential measurements, cLNPs were diluted 1:200 in double-distilled water.

Transmission electron microscopy

A drop of an aqueous solution containing LNPs was placed on a carbon-coated copper grid and dried and analyzed using a JEOL 1200 EX transmission electron microscope.

ASSET LNP incorporation and targeted c-LNP assembly

To incorporate ASSET into LNPs, ASSET was incubated with LNPs for 48 hours at 4°C (1:36, ASSET:RNA weight ratio), as previously described (21). Anti-human EGFR antibody (Bio-Rad Laboratories Inc., clone ICR10) or rat IgG2a isotype control (Bio X Cell, NH, USA, clone 2A3) were used.

LNP quantification and encapsulation

To quantify the RNA in LNPs and to determine the RNA encapsulation efficiency, the Quant-iT RiboGreen RNA assay (Life Technologies) was used as previously described (21, 22). Briefly, 2 μ l of LNPs or dilutions of ribosomal RNA at known concentrations were diluted in a final volume of 100 μ l of TE buffer (10 mM tris-HCl and 20 mM EDTA) in the presence or absence of 0.5% Triton X-100 (Sigma-Aldrich) in a 96-well fluorescent plate (Costar, Corning). The plate was incubated for 10 min at 40°C to allow particles to become permeabilized before adding 99 μ l of TE buffer and 1 μ l of RiboGreen reagent to each well. Plates were shaken at room temperature for 5 min, and fluorescence (excitation wavelength of 485 nm and emission

wavelength of 528 nm) was measured using a plate reader (BioTek Industries) according to the manufacturer's protocol.

LNP transfection

Cells were counted using trypan blue (Biological Industries), and 0.1×10^6 cells were placed in tissue culture 12-well plates (Greiner Bio-One, Germany) with 1 ml of growing medium. MC3 or c-LNPs were added to the wells at RNA amounts of 0.1 to 2 μg . Cells were incubated with the treatments in standard culture conditions for 24 to 120 hours. Then, cells were washed three times, incubated in a fresh culture medium, and collected for flow cytometry (72 to 96 hours) or cell cycle assays (24 to 48 hours), as described below. For 005 cells, cLNPs were preincubated with ApoE3 (0.001 mg/ml; PeproTech, USA) before the addition to the cells.

RNA sequences

sgRNAs were designed and synthesized by Integrated DNA Technologies: GFP, GACCAGGAUGGGCACCACCC/sgRNA core; MmPLK1, CTAGCACCAACACGTCGT/sgRNA core; HsPLK1, AATTACATAGCTCCCGAGGT/sgRNA core. CleanCap Cas9 mRNA (modified) was purchased from TriLink BioTechnologies Inc.

GFP disruption assay

Seventy-two hours after transfection, cells were collected and the percentage of GFP⁻ cells was evaluated using CytoFLEX and analyzed using the CytExpert software (Beckman Coulter, USA).

In vitro uptake experiments

For in vitro uptake experiments, 20% of the total RNA content of cLNPs was replaced with an equal amount of short Cy5.5-labeled DNA oligo (Cy5.5: AGCTCTGTTTACGTCCCAGC). Binding of the labeled cLNPs was assessed by flow cytometry (CytoFLEX and the CytExpert software, Beckman Coulter, USA). Analyses were done with FlowJo software (FlowJo LLC, USA). To determine the uptake of MC3-cLNPs or L8-cLNPs, 0.5×10^6 cells were incubated with cLNPs (0.1 to 1 $\mu\text{g}/\text{ml}$) at 37°C for 2 hours. Cells were collected for flow cytometry analysis after three rounds of PBS wash.

NGS analysis of gene editing

Percentage of gene editing was evaluated in cell lines or sorted tumor cells extracted from tumors (GFP⁺ 005 cells or mCherry⁺ OV8 cells) as described below (single-cell suspension sections). Genomic DNA was extracted with QuickExtract DNA Extraction Solution (Lucigen Inc.) using the manufacturer's protocol, and amplification was performed using locus-specific primers containing universal tails to add sample-unique P5 and P7 indexes for Illumina sequencing in two rounds of polymerase chain reaction (PCR). Following PCR, a 1 \times SPRI (Solid Phase Reversible Immobilization) bead cleanup and library quantification by quantitative PCR (IDT) were performed before sequencing. PCR amplicons were sequenced on an Illumina MiSeq instrument [v2 chemistry; 150-base pair (bp) paired-end reads; Illumina, San Diego, CA, USA]. Data were analyzed using a custom-built pipeline. Data were demultiplexed (Picard tools v2.9; <https://github.com/broadinstitute/picard>); forward and reverse reads were merged into extended amplicons (flash v1.2.11); reads were aligned against the GRCh38 genomic reference (bwa mem v0.7.15), assigned to targets (bedtools tags v2.25). Reads, with more than 30% of bases with quality scores less than 15, were filtered out. At each target, custom python code identified INDELS based on gapped alignments between reads

and targets, and editing was calculated as the percentage of total reads containing an INDEL within an 8-bp window of the cut site.

Cell cycle and cell viability studies

For cell cycle analysis, 5×10^5 cells were collected 48 hours after LNP transfection. The cells were washed with ice-cold PBS and fixed with 70% ethanol for 1 hour. Then, the cells were washed twice with cold PBS and incubated for 10 min at 37°C in 300 μl of PBS with 2-(4-amidinophenyl)-6-indolecarbamidine dihydrochloride (DAPI; 15 $\mu\text{g}/\text{ml}$; Merck KGaA, Darmstadt, Germany). Fluorescence was measured by flow cytometry. Cell viability was evaluated by flow cytometry using APC Annexin V (BioLegend Inc., 640941) and DAPI as recommended by the manufacturer. Data from at least 2×10^4 cells were acquired using CytoFLEX and the CytExpert software (Beckman Coulter, USA). Analyses were done with FlowJo software. For cell cycle analysis, the Dean-Jett-Fox model was applied to at least 10,000 gated cells. Cell viability evaluation was done using the XTT Cell Proliferation Kit (Biological Industries, Israel) according to the manufacturer's recommendation.

005 GBM-bearing mice

Eight-week-old female C57BL/6J OlaHsd mice (Envigo, Rehovot, Israel) were anesthetized, positioned in the Kopf Stereotaxic Alignment System, and inoculated with 3×10^5 005 cells in a 1.5- μl volume using automatic syringe pump in a rate of 0.3 $\mu\text{l}/\text{min}$. Injections were made to the right frontal lobe, ~ 1.5 mm lateral, 2 mm caudal from bregma, and at a depth of 2.3 mm. Bioluminescence imaging (IVIS SpectrumCT, PerkinElmer Inc.) was performed every 5 days after tumor cell implantation to monitor tumor growth. Xenolight D-luciferin (122799, PerkinElmer Inc.) was injected at 15 mg/kg subcutaneously. Bioluminescence analysis was conducted using the Living Image software (PerkinElmer Inc.).

cLNP intracerebral injection

Ten days after tumor inoculation, 005 GBM-bearing mice were anesthetized, positioned in the Kopf Stereotaxic Alignment System, and injected with either sgGFP-cLNPs, sgPLK1-cLNPs, or PBS (0.05 mg/kg) in a 1.5- μl volume using automatic syringe pump in a rate of 0.3 $\mu\text{l}/\text{min}$. Injections were made to the right frontal lobe, ~ 1.5 mm lateral, 2 mm caudal from bregma, and at a depth of 2.3 mm.

Brain single-cell suspensions

Tumor-bearing brains were processed to single-cell suspensions using the Neural Tissue Dissociation Kit (P) (Miltenyi Biotec, USA) and gentleMACS Dissociator according to the manufacturer's protocol. For NGS analysis, GFP⁺ 005 tumor cells were sorted using a BD FACSAria III sorter and further processed as described above.

In vivo tumor distribution

Twenty percent of the total RNA content of the sgGFP-cLNPs was replaced with an equal amount of short Cy5.5-labeled DNA oligo (Cy5.5: AGCTCTGTTTACGTCCCAGC). Four hours after injection, mice were euthanized and brains were harvested. For fluorescent staining, coronal brain sections (40 μm) were cut on a microtome, and images were obtained using a confocal laser-scanning microscope.

OV8-bearing mice

Eight-week-old female Hsd: Athymic Nude-Foxn1nu mice (Envigo, Rehovot, Israel) were injected with 3×10^6 OV8-mCherry cells intraperitoneally. Fluorescence imaging (IVIS SpectrumCT, PerkinElmer

Inc.) was performed weekly after tumor cell implantation to monitor tumor growth. Fluorescence analysis was conducted using the Living Image software (PerkinElmer Inc.).

OV8 tumor single-cell suspensions

Tumor-bearing mice were processed to single-cell suspensions using Tumor Dissociation Kit, mouse (Miltenyi Biotec, USA) and gentleMACS Dissociator, according to the manufacturer's protocol. For NGS analysis, mCherry⁺ tumor cells were sorted using a BD FACSAria III sorter and further processed as described above.

cLNP intraperitoneal injection

OV8-bearing mice were injected intraperitoneally with either anti-EGFR-sgGFP-cLNPs, isotype control-sgGFP-cLNPs, anti-EGFR-sgPLK1-cLNPs, or isotype control-sgPLK1-cLNPs (0.75 mg/kg). For tumor-targeting experiments, OV8-bearing mice were injected intraperitoneally with either anti-EGFR Cy5.5-sgGFP-cLNPs or isotype control Cy5.5-sgGFP-cLNPs (0.75 mg/kg). Fluorescence imaging (IVIS SpectrumCT, PerkinElmer Inc.) was performed 4 hours after LNP injection to evaluate tumor targeting and accumulation. Fluorescence analysis was conducted using the Living Image software (PerkinElmer Inc.).

In vivo toxicity and immunogenicity

Ten-week-old female C57BL/6 mice (Envigo Laboratories) were injected with sgGFP-cLNPs (1 mg/kg) intravenously. Twenty-four hours after injection, blood was collected for biochemistry using Cobas-6000 instrument and complete blood count via Sysmex and ADVIA 120 (A.M.L., Israel). The serum was separated and stored at -80°C before cytokine analysis. Cytokine analysis was done by Pharmaseed Pre-clinical CRO, Israel.

Animal experiments

All animal protocols were approved by the Tel Aviv University Institutional Animal Care and Usage Committee and in accordance with current regulations and standards of the Israel Ministry of Health. All animal experiments were conducted in a double-blinded fashion; the researchers were blinded to group allocation and administered treatments. Mice were randomly divided in a blinded fashion at the beginning of each experiment.

Statistical analysis

Statistical analysis for comparing two experimental groups was performed using two-sided Student's *t* tests. In experiments with multiple groups, one- or two-way analysis of variance (ANOVA) with a Tukey correction was used to calculate differences among multiple populations. Kaplan-Meier curves were used to analyze survival. A value of *P* < 0.05 was considered statistically significant. Analyses were performed with Prism 7 (GraphPad Software). Differences are labeled n.s. for not significant, * for *P* ≤ 0.05, ** for *P* ≤ 0.01, *** for *P* ≤ 0.001, and **** for *P* ≤ 0.0001. Prestablished criteria for the removal of animals from the experiment were based on animal health, behavior, and well-being as required by ethical guidelines.

SUPPLEMENTARY MATERIALS

Supplementary material for this article is available at <http://advances.sciencemag.org/cgi/content/full/6/47/eabc9450/DC1>

[View/request a protocol for this paper from Bio-protocol.](#)

REFERENCES AND NOTES

1. J. Foo, F. Michor, Evolution of acquired resistance to anti-cancer therapy. *J. Theor. Biol.* **355**, 10–20 (2014).
2. S. Hamis, P. Nithiarasu, G. G. Powathil, What does not kill a tumour may make it stronger: *In silico* insights into chemotherapeutic drug resistance. *J. Theor. Biol.* **454**, 253–267 (2018).
3. P. D. Hsu, E. S. Lander, F. Zhang, Development and applications of CRISPR-Cas9 for genome engineering. *Cell* **157**, 1262–1278 (2014).
4. C. A. Vakulskas, D. P. Dever, G. R. Rettig, R. Turk, A. M. Jacobi, M. A. Collingwood, N. M. Bode, M. S. McNeill, S. Yan, J. Camarena, C. M. Lee, S. H. Park, V. Wiebking, R. O. Bak, N. Gomez-Ospina, M. Pavel-Dinu, W. Sun, G. Bao, M. H. Porteus, M. A. Behlke, A high-fidelity Cas9 mutant delivered as a ribonucleoprotein complex enables efficient gene editing in human hematopoietic stem and progenitor cells. *Nat. Med.* **24**, 1216–1224 (2018).
5. Q. Cheng, T. Wei, L. Farbiak, L. T. Johnson, S. A. Dilliard, D. J. Siegwart, Selective organ targeting (SORT) nanoparticles for tissue-specific mRNA delivery and CRISPR-Cas gene editing. *Nat. Nanotechnol.* **15**, 313–320 (2020).
6. L. Zhang, P. Wang, Q. Feng, N. Wang, Z. Chen, Y. Huang, W. Zheng, X. Jiang, Lipid nanoparticle-mediated efficient delivery of CRISPR/Cas9 for tumor therapy. *NPG Asia Mater.* **9**, e441 (2017).
7. Y. K. Tam, T. D. Madden, M. J. Hope, Pieter Cullis' quest for a lipid-based, fusogenic delivery system for nucleic acid therapeutics: Success with siRNA so what about mRNA? *J. Drug Target.* **24**, 774–779 (2016).
8. M. A. Oberli, A. M. Reichmuth, J. R. Dorkin, M. J. Mitchell, O. S. Fenton, A. Jaklenec, D. G. Anderson, R. Langer, D. Blankschtein, Lipid nanoparticle assisted mRNA delivery for potent cancer immunotherapy. *Nano Lett.* **17**, 1326–1335 (2017).
9. E. Senis, C. Fatouros, S. Große, E. Wiedtke, D. Niopek, A.-K. Mueller, K. Börner, D. Grimm, CRISPR/Cas9-mediated genome engineering: An adeno-associated viral (AAV) vector toolbox. *Biotechnol. J.* **9**, 1402–1412 (2014).
10. H. Yin, W. Xue, S. Chen, R. L. Bogorad, E. Benedetti, M. Grompe, V. Kotliansky, P. A. Sharp, T. Jacks, D. G. Anderson, Genome editing with Cas9 in adult mice corrects a disease mutation and phenotype. *Nat. Biotechnol.* **32**, 551–553 (2014).
11. J. D. Finn, A. R. Smith, M. C. Patel, L. Shaw, M. R. Youniss, J. van Heteren, T. Dirstine, C. Cihullo, R. Lescarbeau, J. Seitzer, R. R. Shah, A. Shah, D. Ling, J. Growe, M. Pink, E. Rohde, K. M. Wood, W. E. Salomon, W. F. Harrington, C. Dombrowski, W. R. Strapps, Y. Chang, D. V. Morrissey, A single administration of CRISPR/Cas9 lipid nanoparticles achieves robust and persistent in vivo genome editing. *Cell Rep.* **22**, 2227–2235 (2018).
12. S. Ramishetti, I. Hazan-Halevy, R. Palakuri, S. Chatterjee, S. Naidu Gonna, N. Dammes, I. Freilich, L. Kolik Shmuel, D. Danino, D. Peer, A combinatorial library of lipid nanoparticles for RNA delivery to leukocytes. *Adv. Mater.* **32**, 1906128 (2020).
13. X. Liang, J. Potter, S. Kumar, Y. Zou, R. Quintanilla, M. Sridharan, J. Carte, W. Chen, N. Roark, S. Ranganathan, N. Ravinder, J. D. Chesnut, Rapid and highly efficient mammalian cell engineering via Cas9 protein transfection. *J. Biotechnol.* **208**, 44–53 (2015).
14. S. Kim, D. Kim, S. W. Cho, J. Kim, J.-S. Kim, Highly efficient RNA-guided genome editing in human cells via delivery of purified Cas9 ribonucleoproteins. *Genome Res.* **24**, 1012–1019 (2014).
15. K. J. Kauffman, F. F. Mir, S. Jhunjunwala, J. C. Kaczmarek, J. E. Hurtado, J. H. Yang, M. J. Webber, P. S. Kowalski, M. W. Heartlein, F. DeRosa, D. G. Anderson, Efficacy and immunogenicity of unmodified and pseudouridine-modified mRNA delivered systemically with lipid nanoparticles in vivo. *Biomaterials* **109**, 78–87 (2016).
16. Y. Granot, D. Peer, Delivering the right message: Challenges and opportunities in lipid nanoparticles-mediated modified mRNA therapeutics—An innate immune system standpoint. *Semin. Immunol.* **34**, 68–77 (2017).
17. Y. Fu, J. A. Foden, C. Khayter, M. L. Maeder, D. Reyon, J. K. Joung, J. D. Sander, High frequency off-target mutagenesis induced by CRISPR-Cas nucleases in human cells. *Nat. Biotechnol.* **31**, 822–826 (2013).
18. T. Marumoto, A. Tashiro, D. Friedmann-Morvinski, M. Scadeng, Y. Soda, F. H. Gage, I. M. Verma, Development of a novel mouse glioma model using lentiviral vectors. *Nat. Med.* **15**, 110–116 (2009).
19. D. Friedmann-Morvinski, R. Narasimamurthy, Y. Xia, C. Myskiw, Y. Soda, I. M. Verma, Targeting NF-κB in glioblastoma: A therapeutic approach. *Sci. Adv.* **2**, e1501292 (2016).
20. A. Hallas-Potts, J. C. Dawson, C. S. Herrington, Ovarian cancer cell lines derived from non-serous carcinomas migrate and invade more aggressively than those derived from high-grade serous carcinomas. *Sci. Rep.* **9**, 5515 (2019).
21. R. Mooney, A. A. Majid, J. Batalla-Covello, D. Machado, X. Liu, J. Gonzaga, R. Tirughana, M. Hammad, M. S. Lesniak, D. T. Curiel, K. S. Aboody, Enhanced delivery of oncolytic adenovirus by neural stem cells for treatment of metastatic ovarian cancer. *Mol. Ther. Oncol.* **12**, 79–92 (2018).

22. N. Veiga, M. Goldsmith, Y. Granot, D. Rosenblum, N. Dammes, R. Kedmi, S. Ramishetti, D. Peer, Cell specific delivery of modified mRNA expressing therapeutic proteins to leukocytes. *Nat. Commun.* **9**, 4493 (2018).
23. R. Kedmi, N. Veiga, S. Ramishetti, M. Goldsmith, D. Rosenblum, N. Dammes, I. Hazan-Halevy, L. Nahary, S. Leviatan-Ben-Arye, M. Harlev, M. Behlke, I. Benhar, J. Lieberman, D. Peer, A modular platform for targeted RNAi therapeutics. *Nat. Nanotechnol.* **13**, 214–219 (2018).
24. X. Kang, D. Patel, S. Ng, M. Melchior, Enhanced anti-tumor activity with anti-epidermal growth factor receptor monoclonal antibody cetuximab in combination with carboplatin in preclinical human ovarian carcinoma models. *Mol. Cancer Ther.* **6**, B46 (2007).
25. D. Wang, C. Zhang, B. Wang, B. Li, Q. Wang, D. Liu, H. Wang, Y. Zhou, L. Shi, F. Lan, Y. Wang, Optimized CRISPR guide RNA design for two high-fidelity Cas9 variants by deep learning. *Nat. Commun.* **10**, 4284 (2019).
26. B. P. Kleinstiver, M. S. Prew, S. Q. Tsai, V. V. Topkar, N. T. Nguyen, Z. Zheng, A. P. W. Gonzales, Z. Li, R. T. Peterson, J.-R. J. Yeh, M. J. Aryee, J. K. Joung, Engineered CRISPR-Cas9 nucleases with altered PAM specificities. *Nature* **523**, 481–485 (2015).
27. B. P. Kleinstiver, V. Pattanayak, M. S. Prew, S. Q. Tsai, N. T. Nguyen, Z. Zheng, J. K. Joung, High-fidelity CRISPR-Cas9 nucleases with no detectable genome-wide off-target effects. *Nature* **529**, 490–495 (2016).
28. I. M. Slaymaker, L. Gao, B. Zetsche, D. A. Scott, W. X. Yan, F. Zhang, Rationally engineered Cas9 nucleases with improved specificity. *Science* **351**, 84–88 (2016).
29. D. Wilbie, J. Walther, E. Mastrobattista, Delivery aspects of CRISPR/Cas for in vivo genome editing. *Acc. Chem. Res.* **52**, 1555–1564 (2019).
30. C.-F. Xu, G.-J. Chen, Y.-L. Luo, Y. Zhang, G. Zhao, Z.-D. Lu, A. Czarna, Z. Gu, J. Wang, Rational designs of in vivo CRISPR-Cas delivery systems. *Adv. Drug Deliv. Rev.* (2019).
31. R. Mout, M. Ray, Y.-W. Lee, F. Scaletti, V. M. Rotello, In vivo delivery of CRISPR/Cas9 for therapeutic gene editing: Progress and challenges. *Bioconjug. Chem.* **28**, 880–884 (2017).
32. C. Long, L. Amoasii, A. A. Mireault, J. R. McAnally, H. Li, E. Sanchez-Ortiz, S. Bhattacharyya, J. M. Shelton, R. Bassel-Duby, E. N. Olson, Postnatal genome editing partially restores dystrophin expression in a mouse model of muscular dystrophy. *Science* **351**, 400–403 (2016).
33. C. Long, J. R. McAnally, J. M. Shelton, A. A. Mireault, R. Bassel-Duby, E. N. Olson, Prevention of muscular dystrophy in mice by CRISPR/Cas9-mediated editing of germline DNA. *Science* **345**, 1184–1188 (2014).
34. C. E. Nelson, C. A. Gersbach, Engineering delivery vehicles for genome editing. *Annu. Rev. Chem. Biomol. Eng.* **7**, 637–662 (2016).
35. H. Yin, C.-Q. Song, J. R. Dorkin, L. J. Zhu, Y. Li, Q. Wu, A. Park, J. Yang, S. Suresh, A. Bizhanova, A. Gupta, M. F. Bolukbasi, S. Walsh, R. L. Bogorad, G. Gao, Z. Weng, Y. Dong, V. Kotliansky, S. A. Wolfe, R. Langer, W. Xue, D. G. Anderson, Therapeutic genome editing by combined viral and non-viral delivery of CRISPR system components in vivo. *Nat. Biotechnol.* **34**, 328–333 (2016).
36. H. Li, V. Haurigot, Y. Doyon, T. Li, S. Y. Wong, A. S. Bhagwat, N. Malani, X. M. Anguela, R. Sharma, L. Ivanciu, S. L. Murphy, J. D. Finn, F. R. Khazi, S. Zhou, D. E. Paschon, E. J. Rebar, F. D. Bushman, P. D. Gregory, M. C. Holmes, K. A. High, In vivo genome editing restores haemostasis in a mouse model of haemophilia. *Nature* **475**, 217–221 (2011).
37. R. Mortensen, T. N. Nissen, T. Blauenfeldt, J. P. Christensen, P. Andersen, J. Dietrich, Adaptive immunity against *Streptococcus pyogenes* in adults involves increased IFN- γ and IgG3 responses compared with children. *J. Immunol.* **195**, 1657–1664 (2015).
38. V. L. Simhadri, J. McGill, S. McMahon, J. Wang, H. Jiang, Z. E. Sauna, Prevalence of pre-existing antibodies to CRISPR-associated nuclease Cas9 in the USA population. *Mol. Ther. Methods Clin. Dev.* **10**, 105–112 (2018).
39. A. I. Mehta, A. Linninger, M. S. Lesniak, H. H. Engelhard, Current status of intratumoral therapy for glioblastoma. *J. Neurooncol.* **125**, 1–7 (2015).
40. G. D. Arnone, A. D. Bhimani, T. Aguilar, A. I. Mehta, Localized targeted antiangiogenic drug delivery for glioblastoma. *J. Neurooncol.* **137**, 223–231 (2018).
41. A. Gutkin, Z. R. Cohen, D. Peer, Harnessing nanomedicine for therapeutic intervention in glioblastoma. *Expert Opin. Drug Deliv.* **13**, 1573–1582 (2016).
42. C. Stewart, C. Ralyea, S. Lockwood, Ovarian cancer: An integrated review. *Semin. Oncol. Nurs.* **35**, 151–156 (2019).
43. S. Lheureux, M. Braunstein, A. M. Oza, Epithelial ovarian cancer: Evolution of management in the era of precision medicine. *CA Cancer J. Clin.* **69**, 280–304 (2019).
44. M. Markman, B. Reichman, T. Hakes, J. Curtin, W. Jones, J. L. Lewis Jr., R. Barakat, S. Rubin, B. Mychalczak, P. Saigo, L. Almadrone, W. Hoskins, Intraperitoneal chemotherapy in the management of ovarian cancer. *Cancer* **71**, 1565–1570 (1993).
45. A. Jewell, M. McMahon, D. Khabele, Heated intraperitoneal chemotherapy in the management of advanced ovarian cancer. *Cancers* **10**, 296 (2018).
46. M. E. Skaznik-Wikiel, J. L. Lesnock, W. C. McBee, S. Beriwal, K. K. Zorn, S. D. Richard, T. C. Krivak, R. P. Edwards, Intraperitoneal chemotherapy for recurrent epithelial ovarian cancer is feasible with high completion rates, low complications, and acceptable patient outcomes. *Int. J. Gynecol. Cancer* **22**, 232–237 (2012).
47. R. Jain, J. P. Frederick, E. Y. Huang, K. E. Burke, D. M. Mauger, E. A. Andrianova, S. J. Farlow, S. Siddiqui, J. Pimentel, K. Cheung-Ong, K. M. McKinney, C. Köhrer, M. J. Moore, T. Chakraborty, MicroRNAs enable mRNA therapeutics to selectively program cancer cells to self-destruct. *Nucleic Acid Ther.* **28**, 285–296 (2018).
48. J. Lee, H. Mou, R. Ibrahim, S.-Q. Liang, P. Liu, W. Xue, E. J. Sontheimer, Tissue-restricted genome editing in vivo specified by microRNA-repressible anti-CRISPR proteins. *RNA* **25**, 1421–1431 (2019).
49. B. Shi, E. Keough, A. Matter, K. Leander, S. Young, E. Carlini, A. B. Sachs, W. Tao, M. Abrams, B. Howell, L. Sepp-Lorenzino, Biodistribution of small interfering RNA at the organ and cellular levels after lipid nanoparticle-mediated delivery. *J. Histochem. Cytochem.* **59**, 727–740 (2011).
50. M. M. Weitok, M. E. Zoubek, D. Doleschel, M. Bartneck, M. R. Mohamed, F. Kießling, W. Lederle, C. Trautwein, F. J. Cubero, Lipid-encapsulated siRNA for hepatocyte-directed treatment of advanced liver disease. *Cell Death Dis.* **11**, 343 (2020).

Acknowledgments: We thank N. Dammes for drawing the illustrations and V. Holdengreber for the scientific assistance with electron microscopy. **Funding:** A.G. thanks the Dr. Albert and Doris Fields Trust, the Marian Gertner Institute for Medical Nanosystems, and the Glaser Foundation for her fellowships. This work was supported, in part, by grants from the Israel Cancer Research Fund (grant no. 16-1285-PG). **Author contributions:** D.R., A.G., R.K., S.R., N.V., and D.P. conceived and designed the project. D.R., A.G., A.M.J., M.S.S., and D.F.-M. performed the experimental work. D.R., A.G., A.M.J., M.S.S., D.F.-M., Z.R.C., M.A.B., J.L., and D.P. analyzed the data. D.R., A.G., and D.P. wrote the manuscript. All authors discussed the results. **Competing interests:** A.M.J., M.S.S., and M.A.B. are employed by Integrated DNA Technologies Inc. (IDT), which manufactures reagents similar to some described in the manuscript. M.A.B. owns equity in DHR, the parent company of IDT. R.K. and D.P. are inventors on a patent related to this work filed by Ramot at Tel Aviv University (no. U.S. 10,543,278 B2, published on 28 January 2020). R.K., N.V., and D.P. are inventors on a pending patent related to this work filed by Ramot at Tel Aviv University (no. U.S. 2019/0309087 A1, filed on 10 October 2019). D.P. and S.R. are inventors on a pending patent related to this work filed by Ramot at Tel Aviv University (no. U.S. 2019/0292130 A1, filed on 26 September 2019). D.P., D.R., and A.G. are inventors on a patent application related to this work filed by Ramot at Tel Aviv University (filed on 20 May 2020). **Data and materials availability:** All data needed to evaluate the conclusions in the paper are present in the paper and/or the Supplementary Materials. Additional data related to this paper may be requested from the authors. The ionizable amino lipids and the ASSET linker described in this manuscript can be provided by D.P. pending scientific review and a completed material transfer agreement. Requests for the above materials should be submitted to peer@tauex.tau.ac.il.

Submitted 22 May 2020
Accepted 2 October 2020
Published 18 November 2020
10.1126/sciadv.abc9450

Citation: D. Rosenblum, A. Gutkin, R. Kedmi, S. Ramishetti, N. Veiga, A. M. Jacobi, M. S. Schubert, D. Friedmann-Morvinski, Z. R. Cohen, M. A. Behlke, J. Lieberman, D. Peer, CRISPR-Cas9 genome editing using targeted lipid nanoparticles for cancer therapy. *Sci. Adv.* **6**, eabc9450 (2020).

CRISPR-Cas9 genome editing using targeted lipid nanoparticles for cancer therapy

Daniel Rosenblum, Anna Gutkin, Ranit Kedmi, Srinivas Ramishetti, Nuphar Veiga, Ashley M. Jacobi, Mollie S. Schubert, Dinorah Friedmann-Morvinski, Zvi R. Cohen, Mark A. Behlke, Judy Lieberman, and Dan Peer

Sci. Adv. **6** (47), eabc9450. DOI: 10.1126/sciadv.abc9450

View the article online

<https://www.science.org/doi/10.1126/sciadv.abc9450>

Permissions

<https://www.science.org/help/reprints-and-permissions>

Use of this article is subject to the [Terms of service](#)

Science Advances (ISSN 2375-2548) is published by the American Association for the Advancement of Science. 1200 New York Avenue NW, Washington, DC 20005. The title *Science Advances* is a registered trademark of AAAS.

Copyright © 2020 The Authors, some rights reserved; exclusive licensee American Association for the Advancement of Science. No claim to original U.S. Government Works. Distributed under a Creative Commons Attribution NonCommercial License 4.0 (CC BY-NC).